# Measurement of Lean Blowoff Limits in Swirl-Stabilized Distributed Combustion With Varying Heat Release Intensities

**Rishi Roy**
Department of Mechanical Engineering,
University of Maryland,
College Park, MD 20742
e-mail: rroy1235@umd.edu

**Ashwani K. Gupta**[1]
Department of Mechanical Engineering,
University of Maryland,
College Park, MD 20742
e-mail: akgupta@umd.edu

*Lean blowoff in distributed combustion was investigated at moderate heat release intensities of 5.72, 7.63, and 9.53 MW/m$^3$-atm to characterize the blowoff phenomenon. Distributed combustion conditions were established from a conventional swirl flame at an equivalence ratio of 0.9 using carbon dioxide as the diluent to the inlet airstream. A gradual increase in the air flowrate provided a reduction of equivalence ratio that eventually resulted in the lean blowoff limit. Blowoff occurred at relatively higher equivalence ratios for higher heat release intensities, which was attributed to higher inlet turbulence leading to the early introduction of flame instabilities and blowoff. High-speed chemiluminescence imaging (at 500 frames/second) performed near blowoff moments demonstrated the transition of distributed reaction zone to a near V-shape zone due to quenching of flame surface along the sides. A closer examination of the reduction in equivalence ratio in small steps near the global blowoff showed the presence of a very thin thread-like rotating reaction zone. The observations of blowoff were further supported by the analysis of chemiluminescence signals in each case. The effect of inlet air preheats on blowoff was also investigated. Air preheats broadened the lean blowoff to a lower equivalence ratio which was attributed to enhanced flame speed, providing additional flame stability and reduction of flowfield instabilities. The laminar flame speeds obtained at each preheats case using Chemkin-Pro© simulation with GRI-Mech 3.0 reaction mechanisms supported such a hypothesis of gradually enhanced flame speed, providing additional flame stability.*
[DOI: 10.1115/1.4052795]

*Keywords: distributed combustion, high heat release intensity combustion, lean blowoff, air preheats, laminar flame speed, air emissions from fossil fuel combustion, alternative energy sources, energy conversion/systems, energy extraction of energy from its natural resource, heat energy generation/storage/transfer*

## 1 Introduction

Our quest for a cleaner environment has resulted in increased demands on reducing pollutants emission from power generation that has strongly encouraged the gas turbine manufacturers to focus on cleaner combustion technologies, including lean premixed combustion technology and other novel technologies. However, operating near the lean limits may affect the combustion stability resulting from intense flow and thermal field fluctuations along with local flame blowoff events. While the reduction of pollutant emission is essential during combustion processes, the mitigation of flame instability is crucial to the development of high-performance, efficient gas turbines. Failure to maintain stable combustion may also affect the life of the combustor severely. Hence, the design of any new combustion technologies necessitates closer attention to flame instabilities and blowoff characteristics from fundamental perspectives. Knowledge of lean blowoff provides key insight into the operational limits of combustion technologies that further assist in design modification for stable gas turbine combustor development with ultralow emissions.

Distributed combustion is a novel combustion technology that provides simultaneous benefits of ultralow pollutants emission, fuel flexibility, low noise, wider flammability limits, alleviation of combustion instability, and superior pattern factor (thermal field uniformity) within the combustor [1]. It is based on the principle of high-temperature air combustion technology (called HiTAC) which is now widely used in industrial furnaces. Some similar technologies exist under different names such as moderate or intense low oxygen dilution (MILD) [2] and Flameless Oxidation (FLOX) [3] with slight variations in operating conditions. In MILD combustion, the inlet mixture temperature is higher than its self-ignition temperature and that the maximum temperature rise (with respect to inlet temperature) is lower than the mixture self-ignition temperature. In contrast, the inlet temperature in HiTAC is higher than the self-ignition temperature at much lower oxygen concentration, resulting in a small enhancement of flame temperature during combustion. The FLOX technology relies on injecting high momentum jet flow inlet mixture that generates strong mixing to reduce peak temperatures and $NO_x$ formation. In lab-scale demonstration experiments, distributed combustion is fostered by diluting the main airstream with carbon dioxide, nitrogen, or steam [4]. The hydrodynamic or flow time scale in distributed combustion is much shorter than the chemical time scale so that the Damkohler number < 1 under such condition [5]. The dilution of airstream gradually provides better mixing between the fuel and airstreams and reduces the flame speed as well as the overall flame temperature so that the need for additional air to reduce the flame temperatures is much reduced. In distributed

[1]Corresponding author.

Contributed by the Advanced Energy Systems Division of ASME for publication in the Journal of Energy Resources Technology. Manuscript received October 8, 2021; final manuscript received October 18, 2021; published online November 12, 2021. Editor: Hameed Metghalchi.

combustion, the broadened reaction zone along with the avoidance of hot spots is from the improved mixture preparation of air, fuel, and diluent gases [6]. A uniform low-temperature volumetric reaction zone is established in distributed combustion that assists in reducing the formation of oxides of nitrogen ($NO_x$) and other pollutants.

While the emissions reduction and reaction zone stability characteristics at specific lean equivalence ratios were investigated in the past [7,8], issues such as lean blowoff limits, extinction mechanisms in distributed combustion have not been duly addressed. Studies related to MILD combustions [9] outlined the effect of near blowoff instabilities on pollutant emission (CO concentration) using combined experimental and simulation approaches. The study by Roediger et al. [10] considered lean blowoff in FLOX combustion to demonstrate that the usage of pilot staging may assist in enhancing the operational limit for single-stage combustors. Although these studies discussed the lean blowoff events in relation to their particular technology, the lean blowoff equivalence ratios at various thermal intensity ranges were not reported precisely. Such information is invaluable to understand the characteristics and operational challenges of distributed combustion in realistic operating conditions which operate at higher thermal intensities. Investigation of lean distributed combustion is extremely important to further improve the emission reduction capability of this technology while maintaining operational stability.

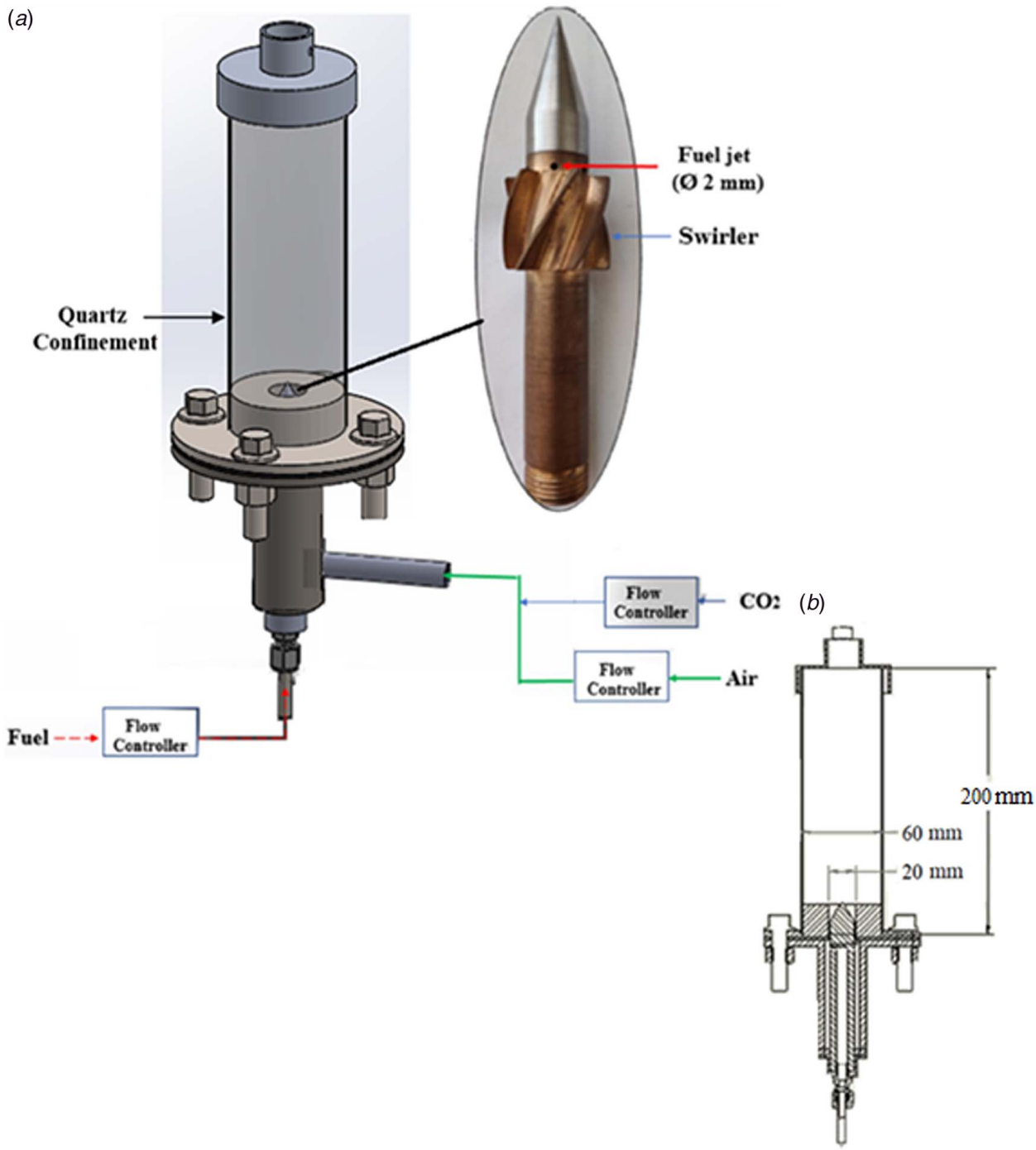


**Fig. 1 (*a*) Sketch of the model experimental swirl combustor (left) and the swirler location in air passageway of the burner (right). (*b*) Cross-sectional view of the burner.**

This paper examines the lean blowoff (LBO) limits in distributed combustion using propane and methane as the fuels at three different heat release intensities (5.72, 7.63, and 9.53 MW/m$^3$-atm). Note that the detailed reaction mechanism study of flame blowoff in distributed combustion was not the focus of this work. Distributed combustion regime was established using a conventional swirl-assisted burner using normal air (at $O_2 \sim 21\%$) at a rather high equivalence ratio of 0.9 (for gas turbine condition) by gradually diluting the inlet airflow with $CO_2$. Next, the airflow rates were varied to reduce the equivalence ratio until reaching the point of blowoff. Lean blowoff equivalence ratios ($\phi_{LBO}$) in distributed combustion were recorded for both the fuels at every examined heat release intensity condition. High-speed chemiluminescence imaging was performed for stable distributed reaction zone conditions (at $\phi = 0.9$) as well as at near blowoff equivalence ratio conditions. The variation of chemiluminescence signal intensities evolved from conventional swirl combustion and distributed combustion (under both stable and near blowoff conditions) was examined at near and far flowfield locations downstream of the burner nozzle exit. Furthermore, the effect of inlet airstream preheats on LBO was investigated at different air preheat temperatures of 400, 600, and 800 K that simulate gas turbine operational conditions. These results were further used to obtain the laminar flame speeds and flame temperatures at the blowoff points corresponding to the examined air preheat temperatures.

## 2 Experimental

Distributed reaction zones during this work were examined using a swirl combustor that also simulates actual hardware encountered in gas turbine combustion. The swirl-assisted burner had a nominal 45-deg swirl angle configuration, and it involved a 20 mm inlet diameter ($D$) nozzle exit that was integrated to a 60 mm internal diameter and 200 mm long outer quartz tube. The calculated swirl number for the swirler was 0.77 [11]. Figure 1 shows a 3D diagram of the model burner as well as its cross-sectional view. Instrument-grade (99.5% pure) propane and chemically pure grade methane was used as the fuels; carbon dioxide was used as the diluent for the air used in this study. The fuel and diluent flow were metered using gravimetric flow controllers (with 1.5% full-scale accuracy). Laminar flow controller (with an accuracy of $\pm 0.8\%$ of reading) was used to control the flow of the primary airstream. The fuel (methane or propane) was directly injected along the longitudinal central axis of the swirler which was then allowed to mix with the main airstream through six equally spaced radial jet holes (of 2 mm diameter) located downstream of the swirler blades. Table 1 demonstrates the various experimental conditions considered during this work.

High-speed chemiluminescence imaging was performed near and far from the point of blowoff using the IDT OS9 high-speed camera that was incorporated with a 50 mm, f/1.8 Nikkor lens and operated at a framing rate of 500 frames/second. Spectral filtering was not applied during imaging to collect the broadband signal. Line-of-sight CH* emission signals were collected using a photomultiplier tube (PMT, Hamamatsu PMT-HC120) with a bandpass filter centered at $430 \pm 10$ nm to detect the blowoff points under operational conditions of distributed combustion. The near blowoff CO and $CO_2$ emissions from the combustion exhaust were measured using a Horiba PG-300 gas analyzer having an accuracy of $\pm 1\%$ of full scale. The CO concentrations (in ppm) were corrected to standard 15% oxygen concentration (with an uncertainty of $\pm 10\%$).

## 3 Results

The results are presented in this section from the different experiments reported with a focus on the fuel-lean condition in swirl-assisted distributed combustion under normal (at $\phi = 0.9$) and near lean blowoff ($\phi_{LBO}$) conditions.

**3.1 Lean Blowoff Limits in Distributed Combustion.** The blowoff equivalence ratios in lean distributed combustion were examined at several different heat release intensities using propane and methane as fuels. In all these cases, distributed combustion was fostered initially at an equivalence ratio of 0.9 and then gradually reduced until approaching the lean blowoff limit. Figure 2 represents the variation of lean blowoff equivalence ratios with different heat release intensities for the two fuels examined. The lean blowoff in distributed combustion using propane fuel occurred at higher equivalence ratios than that for methane fuel at every heat release intensity. Such a difference in blowoff equivalence ratio is attributed to fuel property effects leading to the variation in flame speeds and strain rates [12]. The results show that the lean blowoff ($\phi_{LBO}$) in distributed combustion gradually increased with an increase in heat release intensity for both fuels (see Fig. 2). Such increase in $\phi_{LBO}$ is due to the gradual increase of inlet flow-turbulence intensity that strongly enhanced with higher inlet flowrate at higher heat release intensities. The flow Reynolds numbers at the exit of the burner nozzle were 4992, 6705, 8920 (for methane), and 4886, 6750, 8128 (for propane) corresponding to the 5.72, 6.73, and 9.53 MW/m$^3$-atm heat release intensity. The stability of swirl flames strongly decreases with an increase in turbulence levels that results in global flame extinction at higher equivalence ratios. Besides this, the decrease of flame stability can also be attributed to the heat loss to the burner wall (in this case quartz) from the flame reaction zone resulting in localized flame quenching [13,14]. Higher heat release intensity required higher mass flow of the inlet mixture. Increasing heat release intensity enhanced the heat loss (from the reaction zone) by increased conduction and radiation effects. This paper reports on the role of variation of lean blowoff equivalence ratios in distributed combustion with heat release intensities. It is not the intent here to provide the blowoff mechanism in distributed combustion as it is beyond the scope of this work.

In a previous study [15], $CO_2$ dilution resulted in a gradual drop in adiabatic flame temperature and laminar flame speed when approaching towards distributed combustion similar to Wang et al. [16]. Further dilution (with $O_2 < 16\%$) created an additional drop in flame speed along with the significant fluctuation of the lifted distributed reaction zone. The recent study by Roy and Gupta [8] showed that such fluctuations in the reaction zone of distributed combustion were primarily influenced by the rotational effect of the reaction zone due to the existence of precessing vortex core (PVC) [17–19]. Such instabilities of reaction zone were seen to finally lead to global blowoff under fuel-lean conditions.

**Table 1 Experimental conditions**

| Heat release intensity (MW/m$^3$-atm) | Propane flowrate (L/min) | Methane flowrate (L/min) | Diluent $CO_2$ flowrate (L/min) | | Air flowrate (L/min) | |
|---|---|---|---|---|---|---|
| | | | For propane | For methane | For propane | For methane |
| 5.72 | 2 | 4.93 | 12 | 11.50 | 52 | 51 |
| 7.63 | 2.67 | 6.57 | 16.50 | 16 | 72 | 68 |
| 9.53 | 3 | 8.50 | 18.50 | 20 | 88 | 92 |

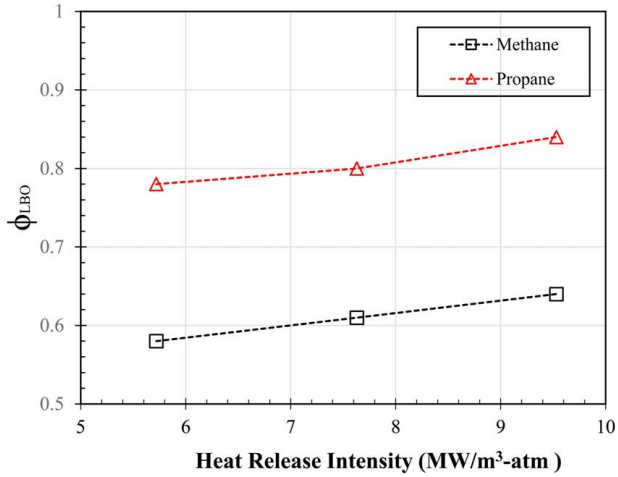


**Fig. 2 Lean blowoff equivalence ratio at different heat release intensities in distributed combustion using propane and methane fuels**

**3.2 Chemiluminescence Imaging Near and Away From Blowoff.** Imaging of broadband flame chemiluminescence was conducted for both conventional swirl combustion and distributed combustion at various heat release intensities. Figure 3 shows the average chemiluminescence images. The top row of Fig. 3 shows the normal stable swirl combustion (at $\phi = 0.9$) while the bottom row shows corresponding distributed reaction zones, both using propane as the fuel. These images represent time-averaged signatures from 500 consecutive images. The results show that the reaction zone becomes wider and elongated with an increase in the thermal intensity of the swirl flames. The inner recirculation zone (IRZ) was also relatively longer for higher thermal intensity flames. In contrast to conventional combustion, distributed reaction zones spanned almost over the entire volume of the burner having lower chemiluminescence intensity than normal swirl flames. Such reduction of visible signature occurred primarily due to the reduction of adiabatic flame temperature with gradual $CO_2$ dilution [8]. The gradient of the observed chemiluminescence signal (across the regular swirl flame) was remarkably decreased in distributed combustion. With the increase in thermal intensity, the distributed reaction zones acquired gradually larger combustor volume and the flames were attached relatively closer to the nozzle exit. A very similar observation was made (in normal air combustion and distributed combustion) when methane was used as the fuel.

Chemiluminescence imaging was further performed to capture the near blowoff behavior in distributed reaction zones. Such observations help in characterizing the behavior of distributed reaction zones near global extinction. Figure 4 shows sample instantaneous images near blowoff for the heat release intensity of 9.53 MW/m$^3$-atm under distributed reaction condition near to just above and very close to blowoff $\phi_1 = \phi_{LBO} + 0.06$ (top row) and $\phi_2 = \phi_{LBO} + 0.02$ (bottom row). The images in each row are not consecutive so that they reveal some characteristic structures at the given conditions. Significant quenching along the right and left sides of the reaction zone at $\phi_1$ resulted in a change of flame shape from distributed to near V-shape. The middle image (of the top row) shows more overall volume of the reaction zone while the rightmost image shows a significantly quenched reaction zone leading to much-reduced volume. Such alteration of shapes of the reaction zone was periodic and sustained without global extinction. Due to further quenching, the reaction zone appeared as a thin (thread-like) behavior with significant standoff height at $\phi_2$. Different shapes represented at $\phi_2$ showed a similar thin revolving reaction zone with some bending observed at the flame base of the reaction zone as seen from the middle image at $\phi_2$. Localized wrinkling of flame surfaces (on both sides) was clearly observed possibly due to the complex interaction between vortical structures with the reaction zone, heat release fluctuations, and helical instabilities [20]. However, further appropriate understanding of such an event requires non-intrusive planar laser-based investigations of such complex flowfields. Further reduction of $\phi$ resulted in global blowoff of reaction zone at $\phi_{LBO}$. Nearly similar observations were also made of the blowoff moments at lower heat release intensities except that the reaction zones observed at $\phi_1$ and $\phi_2$ were relatively thin and shorter in length. The near-field (at $y = 25$ mm) and

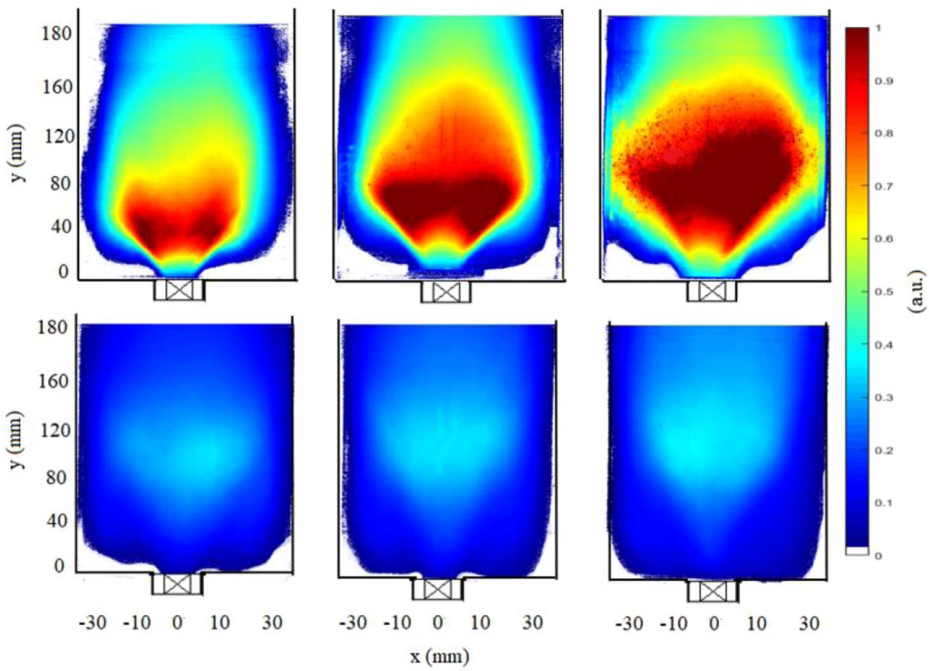


**Fig. 3 Average of 500 chemiluminescence images of stable swirl combustion (at $\phi = 0.9$) (top row) and distributed combustion (bottom row) at heat release intensities of 5.72, 7.63, and 9.53 MW/m$^3$-atm using propane fuel**

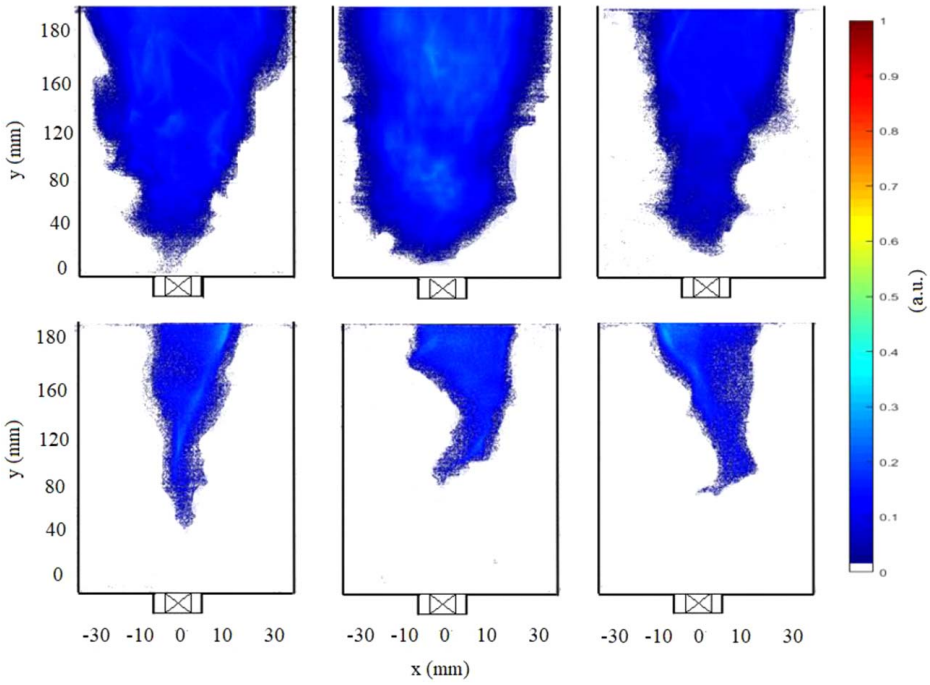


**Fig. 4 Instantaneous chemiluminescence images near to blowoff. Top row at $\phi LBO + 0.06$, and bottom row at $\phi_{LBO} + 0.02$ using propane fuel (at heat release intensities of 9.53 MW/m$^3$-atm).**

far-field (at $y = 135$ mm) chemiluminescence signal intensity were also examined for 9.53 MW/m$^3$-atm flame to characterize the lean blowoff event. Figure 5 shows such signal variation across the reaction zone in conventional swirl combustion, distributed combustion (at $\phi = 0.9$), and at near blowoff equivalence ratio conditions. Such intensity distribution was obtained from chemiluminescence strips of one-pixel thickness spanned across the reaction zone (from left to right). In the near-field, the swirl flame demonstrated a steep signal gradient on both sides of the flame. Two distinguished peaks observed at the top of the swirl flame's signal profile are attributed to the peak heat release zones. In contrast, the signal intensity in distributed combustion was remarkably lower and relatively uniform across the reaction zone. The small central peak in distributed reaction zone signified slightly more heat release near that zone. The noticeable reduction of signal intensity can be observed near blowoff equivalence ratio conditions. The small centrally located peak at $\phi_1$ indicated sidewise quenching of most of the reaction zone while the completely diminished chemiluminescence signal at $\phi_2$ occurred due to extinguished reaction zone at that location. The far-field chemiluminescence manifested a very uniform signal intensity across the distributed reaction zone. Note that the magnitude of the signal in normal swirl combustion was lower than that of the distributed combustion (at $\phi = 0.9$) in the far-field. This is because the heat release in swirl flame (at $O_2 = 21\%$) primarily occurred at locations of between $y = 30$ and 90 mm. Hence, lower chemiluminescence intensity was recorded for the

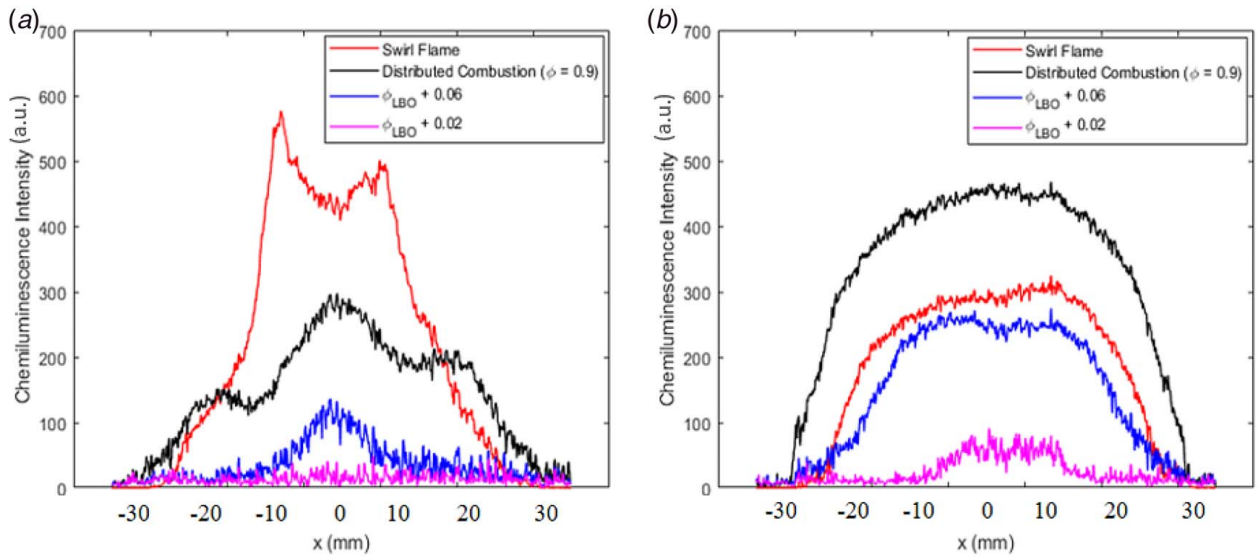


**Fig. 5 Radial distribution of chemiluminescence intensity at (*a*) near-burner exit flowfield (at $y = 25$ mm) and (*b*) farther away flowfield (at $y = 135$ mm) using propane fuel (at heat release intensities of 9.53 MW/m$^3$-atm)**

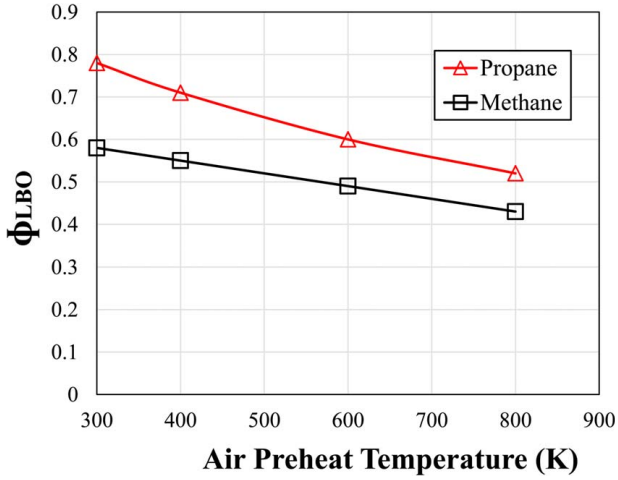


**Fig. 6 Lean blowoff equivalence ratio of propane and methane flames (at 5.72 MW/m$^3$-atm heat release intensity) with $CO_2$ dilution at different air preheat temperatures**

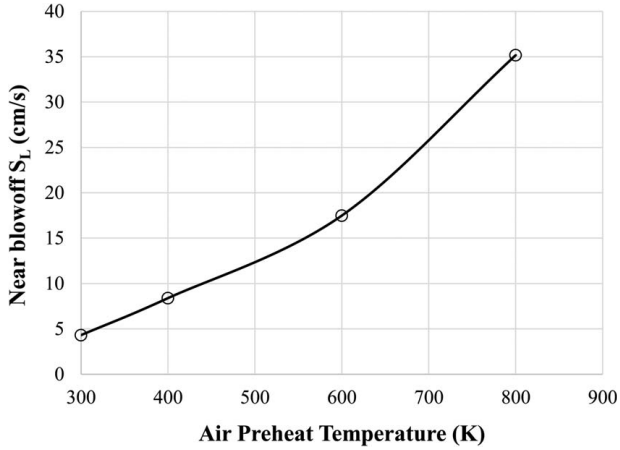


**Fig. 7 Laminar flame speed ($S_L$) near blowoff ($\phi_{LBO}+0.02$) for methane fuel at different air preheat temperatures**

conventional swirl flame in the far-field. At $\phi_1$ considerable chemiluminescence was noticed in the far-field, unlike the near-field. This confirms the existence of a lifted volumetric reaction zone with a nearly extinguished base (close to the nozzle exit). A similar observation can be made at $\phi_2$ although with much-reduced chemiluminescence signal. Similar observations of chemiluminescence distribution were made at other heat release intensities examined here.

**3.3 Effect of Preheating on Blowoff.** The effect of air preheats with $CO_2$ dilution was investigated to understand its effect on $\phi_{LBO}$ of distributed reaction zones, the possible influence of a flame. The experimental conditions for distributed combustion (at $\phi = 0.9$) were kept constant while the inlet airstream was preheated to 400, 600, and 800 K, respectively. Preheating of airstream up to 800 K was performed to keep the adiabatic flame temperature ($T_{ad}$) of distributed reaction zones constant [8]. Reduction of $\phi$ was carried out until reaching the blowoff conditions at different heat release intensities. Figure 6 shows the variation $\phi_{LBO}$ at different air preheat temperatures for the 5.72 MW/m$^3$-atm thermal intensity flame using both propane and methane fuel. The $\phi_{LBO}$ gradually reduced with an increase in preheat temperatures of the inlet airstream for both cases. Such observation is reasonable and as expected since air preheats of inlet air enhanced the laminar flame speed [21–23] that provided additional stability to the reaction zone. Hence, the flame is sustained for a longer period of time with gradual preheating. The enhancement of reaction zone stability with preheating also indicates that the significant drop in flame temperature (due to $CO_2$ dilution) is an important factor governing the lean blowoff events in distributed combustion. Thus, the distributed flames were extinguished at relatively lower equivalence ratios (than the non-preheated case) when preheating was applied to raise the temperature of reaction zones. Similar results of gradually lowering blowoff equivalence ratios with preheat temperatures were observed for other heat release intensities. To corroborate the hypothesis of enhanced flame speed, the laminar flame speed ($S_L$) and the adiabatic flame temperature ($T_{ad}$) were further calculated using Chemkin-Pro simulation coupled with GRI-Mech 3.0 [24] using the sample case for methane fuel. GRI-Mech 3.0 considers 53 chemical species and 325 chemical reactions during these calculations. Figures 7 and 8 show the variations of near blowoff (at $\phi_2$) laminar flame speed ($S_L$) and adiabatic flame temperature ($T_{ad}$) for methane fuel at the three different air preheat temperatures considered in this study. The results show that near blowoff $S_L$ gradually increased with the increase in air preheat temperatures. The growth of $S_L$ at higher air preheat temperatures (600–800 K) was faster than initial air preheats (~400 K). This observation is convincing as the change in $S_L$ is impacted simultaneously by both the dilution effect of $CO_2$ and air preheats. The slower initial growth rate of $S_L$ is primarily due to the influence of $CO_2$ dilution over air preheats. As the air preheat temperature was increased, the thermal dissociation of $CO_2$ took place. Hence, the effect of air preheats on $S_L$ becomes more dominant than that of the $CO_2$ dilution.

The competing effects between $CO_2$ dilution and preheating can also be observed from the variations in $T_{ad}$ shown in Fig. 8. Up to 400 K, the predominance of $CO_2$ dilution tends to weaken the air preheat effect on flame temperature. The drop in $\phi$ (by increasing the airflow) to attain LBO provided an additional reduction of flame temperature. Hence, such decrease of $T_{ad}$ continued till ~400 K. After 400 K, the flame temperature started rising again due to the increased influence of air preheats over $CO_2$ dilution effects. To verify this hypothesis of thermal decomposition of $CO_2$ at higher air preheat temperatures, the concentrations of near blowoff CO and $CO_2$ in the exhaust were measured experimentally (using a gas analyzer) as well as with Chemkin-Pro© simulation. Figure 9 demonstrates the mole fraction of CO and $CO_2$ (both measured and calculated) near blowoff (at $\phi_2$) at various air preheats temperature reported. When the concentration of $CO_2$ systematically went down with the increase in preheats, the CO concentration (ppm) increased at temperatures higher than 600 K. This observation was consistent between experimental measurement and

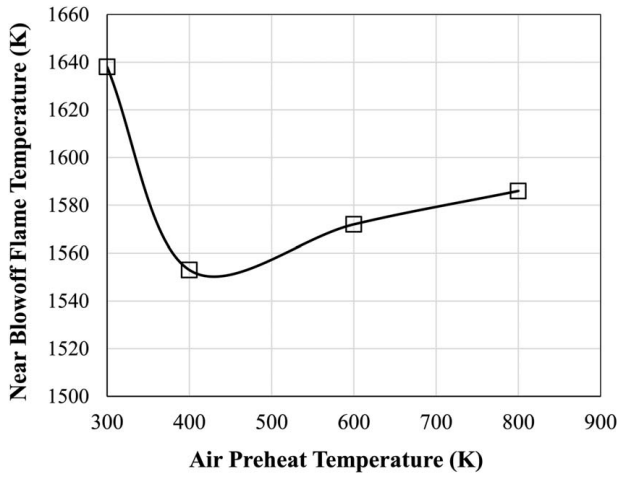


**Fig. 8 Adiabatic flame temperature ($T_{ad}$) near blowoff ($\phi_{LBO}+0.02$) of methane flame for three different air preheat temperatures**

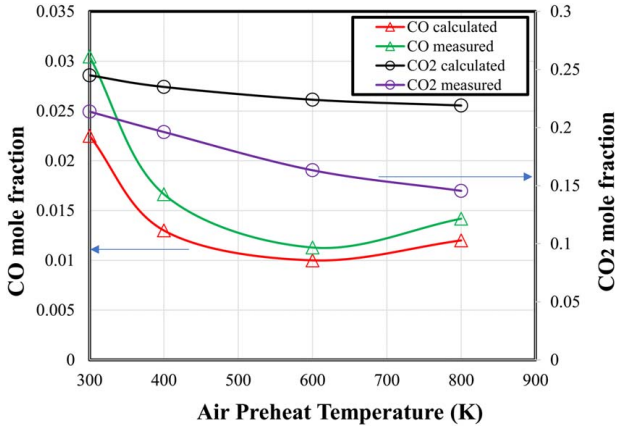


**Fig. 9 CO and $CO_2$ concentrations near blowoff ($\phi_{LBO} + 0.02$) at different air preheat temperatures**

Chemkin-Pro© simulation results. Such results support the high-temperature decomposition of $CO_2$ that occurred at high air preheat temperatures in the range 600–800 K. Note that the difference in magnitudes of mole fractions (of CO and $CO_2$) between experimental and simulation results occurred mainly due to the difference in the number of species considered for such calculation. While the Chemkin-Pro© considered 53 species, the gas analyzer reported only six key species in the exhaust. However, the trend of variations of near blowoff CO and $CO_2$ mole fractions with preheat temperatures were similar for both experimental measurement and simulation. Similar trends of near blowoff flame speed and temperature were also observed for propane fuel.

The reduction of LBO equivalence ratio with air-preheats for this particular burner is also related to enhanced stability of reaction zone as observed in our previous study [8]. The instabilities in this current swirl-burner arise primarily due to thermo-acoustic coupling and the existence of PVC. It was observed that preheating of inlet airstream helped in significantly reducing the amplitude of heat release fluctuation (resulting in dampening of thermo-acoustic nature) and the PVC peak frequency in power spectral density (PSD) plots. Reduction of such instability peaks helps in restoring the stability reaction zones. Similar enhancement of stability of distributed reaction zone occurred due to preheating effects as compared to non-preheated cases near blowoff [25]. Hence, the suppression of flowfield instabilities due to air preheats also played an important role in extending the life of distributed combustor by decreasing the LBO equivalence ratios. Additionally, the increase in air preheats gradually decreased the flow Reynolds number that resulted in the reduction of inlet turbulence intensity [26]. Such reduction of turbulence intensity also helped in the reduction of inherent instabilities such that the flame was sustained for a longer period.

## 4 Conclusions

Lean blowoff in distributed combustion was investigated using propane and methane fuels at three different heat release intensities of 5.72, 7.63, and 9.53 MW/$m^3$-atm in a swirl-assisted combustor. Distributed combustion was fostered from conventional swirl flames ($O_2 = 21\%$) at an equivalence ratio ($\phi$) 0.9 by diluting the main airstream with $CO_2$. The $\phi$ was reduced by increasing the inlet airflow for each case. High-speed chemiluminescence signatures (performed at 500 frames/second) showed large and relatively wider reaction zones both in swirl combustion and in distributed combustion, although the reaction zone was much wider in distributed combustion than swirl combustion. Near LBO, significant quenching of distributed reaction zone led to nearly a V-shape (at $\phi_{LBO} + 0.06$) and thin thread-like shape with a further reduction of ϕ (at $\phi_{LBO} + 0.02$). The LBO $\phi$ increased gradually with an increase in heat release intensity, which was attributed to higher flowfield instability due to enhanced inlet turbulence. Analysis of chemiluminescence signals at near and far-field locations (at $y =$ 25 mm and 135 mm) of the flames helped to characterize the lean blowoff of the flames. Such signal variation confirmed the existence of lifted reaction zones at $\phi_{LBO} + 0.06$ while a heavily quenched thin reaction zone was inferred at $\phi_{LBO} + 0.02$. These results support the observations made from chemiluminescence images near the blowoff conditions. The effect of air preheats on LBO of $CO_2$ diluted reaction zones was also investigated. Air preheats helped to extend the blowoff event to a lower equivalence ratio than no air preheats. Such decrease in LBO $\phi$ was primarily due to the additional flame stability (and enhanced flame speed) gained with air preheats. Calculation of laminar flame speed ($S_L$) and adiabatic flame temperature ($T_{ad}$) using Chemkin code with GRI-Mech 3.0 confirmed the gradual increase of near blowoff $S_L$ with an increase in air preheats temperature. However, the initial steep decrease in $T_{ad}$ (near blowoff) up to 400 K was primarily due to the predominant effect of $CO_2$ dilution over the air preheat effect. Above 400 K, high-temperature dissociation of $CO_2$ becomes an important factor leading to the weakened effect of dilution on $T_{ad}$ reduction. This resulted in increased $T_{ad}$ (for air preheats above 400 K) due to the stronger influence of air preheats over the chemical effect. This hypothesis of high-temperature decomposition of $CO_2$ was supported from the CO and $CO_2$ mole fractions measurements (with experiment and simulation) near blowoff at different air preheat temperatures. Furthermore, air preheats assisted in significantly reducing the amplitude of heat release fluctuation and the PVC peak frequency resulting in dampening of thermo-acoustic coupling and hydrodynamic instabilities in the examined burner. Such reduction of instabilities helped in extending the LBO to lower equivalence ratios compared to non-preheated cases.

## Acknowledgment

This research was supported by the Office of Naval Research (ONR), USA and is gratefully acknowledged by the authors.

## Conflict of Interest

There are no conflicts of interest.

## Data Availability Statement

The datasets generated and supporting the findings of this article are obtainable from the corresponding author upon reasonable request. The authors attest that all data for this study are included in the paper. Data provided by a third party listed in Acknowledgment. No data, models, or code were generated or used for this paper.

## References

[1] Khalil, A. E. E., and Gupta, A. K., 2104, "Velocity and Turbulence Effect on High Intensity Distributed Combustion," Appl. Energy, **125**(1), pp. 1–9.
[2] Lammel, O., Schutz, H., Schmitz, G., Luckerath, R., Stohr, M., Noll, B., Aigner, M., Hase, M., and Krebs, W., 2010, "FLOX® Combustion at High Power Density and High Flame Temperature," ASME J. Eng. Gas Turbines Power, **132**(12), p. 121503.
[3] Cavaliere, A., and De Joannon, M., 2004, "Mild Combustion," Prog. Energy Combust. Sci., **30**(4), pp. 329–366.
[4] Khalil, A. E. E., and Gupta, A. K., 2017, "Acoustic and Heat Release Signatures for Swirl Assisted Distributed Combustion," Appl. Energy, **193**(1), pp. 125–138.
[5] Hampp, F., Kraus, P., Simatos, P., and Lindstedt, R. P., 2016, "Distributed Low Temperature Combustion: Fundamental Understanding of Combustion Regime Transitions," Final Report FA8655-13-1-3024, AFRL-AFOSR-UK-TR-2016-0021, Imperial College London.
[6] Arghode, V. K., Gupta, A. K., and Bryden, K. M., 2012, "High Intensity Colorless Distributed Combustion for Ultra-low Emissions and Enhanced Performance," Appl. Energy, **92**(1), pp. 822–830.
[7] Khalil, A. E. E., and Gupta, A. K., 2016, "Fuel Property Effects on Distributed Combustion," Fuel, **171**(1), pp. 116–124.

[8] Roy, R., and Gupta, A. K., 2021, "Experimental Investigation of Flame Fluctuation Reduction in Distributed Combustion," Exp. Fluids, **62**(4), p. 62.
[9] Zhang, H., Zhang, Z., Xiong, Y., Liu, Y., and Y, X., 2018, "Experimental and Numerical Investigations of MILD Combustion in a Model Combustor Applied for Gas Turbine," Proceedings of ASME Turbo Expo Turbomachinery Technical Conference and Exposition, Oslo, Norway, June 11–15, Paper No. GT2018-76253.
[10] Roediger, T., Lammel, O., Aigner, M., Beck, C., and Krebs, W., 2013, "Part-Load Operation of a Piloted FLOX® Combustion System," ASME J. Eng. Gas Turbines Power, **135**(3), p. 031503.
[11] Khalil, A. E. E., Brooks, J. M., and Gupta, A. K., 2016, "Impact of Confinement on Flowfield of Swirl Flow Burners," Fuel, **184**(1), pp. 1–9.
[12] Palacios, A., Bradley, D., and Hu, L., 2016, "Lift-Off and Blow-Off of Methane and Propane Subsonic Vertical Jet Flames, With and Without Diluent Air," Fuel, **183**(1), pp. 414–419.
[13] Yang, X., Yang, W., Dong, S., and Tan, H., 2020, "Flame Stability Analysis of Premixed Hydrogen/Air Mixtures in a Swirl Micro-combustor," Energy, **209**(1), p. 118495.
[14] Wang, Z., Hu, B., Fang, A., Zhao, Q., and Chen, X., 2021, "Analyzing Lean Blow-Off Limits of Gas Turbine Combustors Based on Local and Global Damköhler Number of Reaction Zone," Aerosp. Sci. Technol., **111**(1), p. 106532.
[15] Roy, R., and Gupta, A. K., 2020, "Flame Structure and Emission Signature in Distributed Combustion," Fuel, **262**(1), p. 116460.
[16] Wang, Z., Yelishala, S. C., Yu, G., Metghalchi, H., and Levendis, Y. A., 2019, "Effects of Carbon Dioxide on Laminar Burning Speed and Flame Instability of Methane/Air and Propane/Air Mixtures: A Literature Review," Energy Fuels, **33**(10), pp. 9403–9418.
[17] Syred, N., Gupta, A. K., and Beér, J. M., 1975, "Temperature and Density Gradient Changes Arising With the Processing Vortex Core and Vortex Breakdown in Swirl Burners," Proceedings of the 15th Symposium (Intl.) on Combustion, Tokyo, Japan, Aug. 25–31, 1974, The Combustion Institute, pp. 587–597.
[18] Syred, N., Hanby, V. I., and Gupta, A. K., 1973, "Resonant Instabilities Generated by Swirl Burners," J. Inst. Fuel, **46**(387), pp. 402–407.
[19] Mardani, A., Rekabdarkolaei, B. A., and Rastaaghi, H. R., 2020, "Experimental Investigation on the Effects of Swirlers Configurations and Air Inlet Partitioning in a Partially Premixed Double High Swirl Gas Turbine Model Combustor," ASME J. Energy Resour. Technol., **143**(1), p. 012302.
[20] Acharya, V. S., Shin, D. H., and Lieuwen, T., 2013, "Premixed Flames Excited by Helical Disturbances: Flame Wrinkling and Heat Release Oscillations," J. Propul. Power, **29**(6), pp. 1282–1291.
[21] Elia, M., Ulinski, M., and Metghalchi, M., 2001, "Laminar Burning Velocity of Methane–Air–Diluent Mixtures," ASME J. Eng. Gas Turbines Power, **123**(1), pp. 190–196.
[22] Rahim, F., Far, K., Parsinejad, F., Andrews, R., and Metghalchi, H., 2008, "A Thermodynamic Model to Calculate Burning Speed of Methane-Air-Diluent Mixtures," Int. J. Thermodyn., **11**(4), pp. 151–160.
[23] Yelishala, S. C., Wang, Z., Metghalchi, H., Levendis, Y. A., Kannaiyan, K., and Sadr, R., 2019, "Effect of Carbon Dioxide on the Laminar Burning Speed of Propane–Air Mixtures," ASME J. Energy Resour. Technol., **141**(8), p. 082205.
[24] Smith, G. P., Golden, D. M., Frenklach, M., Moriarty, N. W., Eiteneer, B., Goldenburg, M., Bowman, C. T., et al., 1999, "GRI 3.0 Mechanism," http://www.me.berkeley.edu/gri_mech/
[25] Khalil, A. E. E., Gupta, A. K., Bryden, K. M., and Lee, S. C., 2020, "Mixture Preparation Effects on Distributed Combustion for Gas Turbine Applications," ASME J. Energy Resour. Technol., **134**(3), p. 032201.
[26] Yue, H., Guo-Biao, C., Hai-Xing, W., Bruno, R., and Abdelkrim, B., 2014, "Flow Characterization and Dilution Effects of N2 and CO2 on Premixed CH4/Air Flames in a Swirl-Stabilized Combustor," Chin. Phys. B, **23**(3), p. 034704.